Supporting Information

Ostermaier et al. 10.1073/pnas.1319402111

SI Materials and Methods

Preparation of Rhodopsin in Rod Outer Segments. Rod outer segments (ROS) were prepared from bovine retinas under dim red light as described (1). In detail, 200 frozen retinas were covered with 100 mL ice-cold buffer A [10 mM Tris (pH 7.4), 150 mM KCl, 2 mM $MgCl_2$, 1 mM EDTA, 2 mM β-mercaptoethanol, 1 mM PMSF, and protease inhibitor mixture Roche Complete] containing 34.2% (wt/vol) sucrose and slowly thawed. The suspension was bubbled with argon, vigorously shaken, and then centrifuged at 2,750 × *g* for 30 min at 4 °C (Heraeus Multifuge X3R, swinging bucket rotor TX-750; Thermo Scientific). The supernatants were pooled and expanded with sucrose buffer to a volume of 400 mL, mixed, and centrifuged in six tubes (type 45 Ti) at 22,800 × *g* for 30 min at 4 °C. The pelleted crude ROS were resuspended in a total of 120 mL buffer A and distributed to six tubes (type SW28). Each sample was underlayered with 8 mL buffer A containing 31.5% (wt/vol) sucrose and 8 mL buffer A containing 34.2% (wt/vol) sucrose. After centrifugation at 53,000 × *g* (Optima XL-100K Ultracentrifuge; Beckman Coulter) for 30 min at 4 °C, pure ROS enriched in a single band were harvested and mixed with an equal volume of buffer A. ROS were recovered by centrifugation at 23,000 × *g* for 30 min at 4 °C. Pellets were resuspended in buffer A and then stored in the dark at −80 °C.

Phosphorylation of Rhodopsin in ROS. Rhodopsin was phosphorylated in ROS membranes essentially as described (2), yielding a mixture of rhodopsin species containing any number of phosphates up to seven phosphate groups per molecule with three phosphates sufficient for high-affinity rhodopsin binding (3). Briefly, ∼10 μM rhodopsin in ROS, 5 mM ATP, and 20 μM GTP were mixed in a total volume of 400 mL buffer B [100 mM potassium phosphate (pH 7.0), 5 mM $MgCl_2$, 0.1 mM EDTA, 2 mM β-mercaptoethanol, 0.5 mM PMSF, and complete protease inhibitor mixture Roche], sonicated for 2 min in a water bath, and then illuminated [highest intensity; Lite Mite Imagelite (Stocker & Yale)] for 2 h at 30 °C while stirring gently.

Dark-state rhodopsin was regenerated with a 3.2-fold excess of 9-*cis*-retinal overnight. Regenerated phosphorylated ROS (P-ROS) were pelleted by centrifugation at 49,000 × *g* for 30 min at 4 °C. To remove free retinal, ROS were washed once in 400 mL buffer B supplemented with 50 mM hydroxylamine and 2% (wt/vol) BSA, twice in buffer B with 2% (wt/vol) BSA, and three times in buffer C [10 mM Hepes (pH 7.0), 100 mM NaCl, 1 mM DTT, 1 mM $MgCl_2$, and 0.1 mM EDTA]. The concentration of rhodopsin was measured by the loss of absorbance at 485 nm (ε = 40,800 $M^{-1}{\cdot}cm^{-1}$) (4) following illumination of ROS membranes and was adjusted to 1–1.5 mg/mL rhodopsin in buffer C. Aliquots were stored in the dark at −80 °C.

Scanning Mutagenesis. Bovine arrestin-1 was cloned into the EgWoMiPi vector for expression in bacterial and mammalian cells (Fig. S4). Primers for the scanning mutagenesis were designed using the program AAscan (5). Briefly, 1× Phusion High-Fidelity PCR master mix with GC buffer (Thermo Scientific) was complemented with 400 mM 3-trimethylsilyl-2-oxazolidinone and 170 pg DNA template per reaction and then distributed to a 96-well microplate in 17-μL portions. Then, 1.5 μL each of 1-μM forward and reverse primers were added to each well. The PCR product was treated with DpnI overnight to remove the methylated template DNA. The resulting product was transformed into *Escherichia coli* strain Mach1 and plated. A single colony of each mutant was transferred to a 96-well agar plate with appropriate antibiotics and sent for sequencing to GATC Biotech. The sequence was checked using the program MutantChecker. Programs used for scanning mutagenesis are available at (www.psi.ch/lbr/aascan).

Arrestin Expression. Arrestin mutants were expressed in *E. coli* strain BL21(DE3) in sets of 12 each including wild type as reference for relative expression levels. For each mutant, a preculture of 4 mL LB complemented with 50 μg/mL Kanamycin was inoculated with several colonies, shaken overnight at 37 °C, and then diluted 1:50 in 100 mL LB media. *E. coli* cultures were grown until an OD_{590} of 0.6–0.8, then 0.5 mM IPTG was added, and expression allowed for about 20 h. Cells were pelleted at 4,800 × *g* for 10 min at 4 °C and stored at −80 °C.

For comparison of arrestin mutants, cell pellets from 50 mL-cultures were resuspended with 1.2 mL ice-cold buffer C containing 0.2 mg/mL lysozyme, 20 μg/mL DNase, 1.5 mM PMSF, and protease inhibitor mixture Roche Complete. Samples were sonicated using a chilled 96-well sonicator head [3-min pulse (3 s on and 3 s off) and amplitude 80% (Vibra Cell VCX 600; Sonics)]. After cell disruption the samples were centrifuged at 21,100 × *g* (Centrifuge 5424R; Eppendorf) for 1 h at 4 °C and the cleared cell lysate was used for the rhodopsin binding assays described below.

Direct Binding Assay. Per day, three sets containing 11 arrestin mutants and one wild-type control were analyzed in parallel using a 96-well centrifugal pull-down assay (Fig. S1). The 36 master mixes were prepared by combining 1,024 μL cleared cell lysate of each mutant arrestin with 76 μL (1.45 mg/mL) P-ROS or ROS, respectively.

For comparison of arrestin mutants, we distributed 100-μL portions of each master mix on 96-well plates (twin.tec PCR plate 96, skirted; Eppendorf). Rows A–H were prefilled with 100 μL buffer C containing increasing amounts of sodium chloride for final concentrations of 100, 247, 492, 737, and 982 mM and 1.472, 1.962, and 2.403 M NaCl, respectively. The contents of each well were mixed, incubated at 37 °C for 5 min, and light activated for 6 min (highest intensity, 495-nm long-pass filter; Lite Mite Imagelite). One 100-μL portion of each master mix was combined with 100 μL buffer C in a separate 96-well plate and used as a dark control.

After light activation, the 96-well plates were centrifuged at 6,168 × *g* [HIGHPlate 6000 microplate rotor (Thermo Scientific)] for 20 min at 4 °C to pellet the suspended ROS membranes. Supernatants were removed by inverting the plates. One hundred microliters of buffer C were added to each sample without disturbing the pellets and centrifugation was repeated. Inverting the plates and centrifuging the inverted plates with precision wipes underneath at 300 × *g* for 15 s removed supernatants completely. Pellets were resuspended with each 100 μL buffer C (using VIAFLO 96; Integra Biosciences) and transferred into 96-well plates [FLUOTRAC 600, flat-bottom, black(USA Scientific)]. Fluorescence intensity was quantified in a microplate reader (Tecan Safire2, program Magellan). The fluorescence values were normalized (from 0% to 100%) within each set of measurements. The data were fitted to sigmoidal dose–response curves with variable slope (Eq. **S1**) in Prism (GraphPad) to extract the half-maximal inhibitory concentrations (IC_{50}). IC_{50} and R^2 values, 95% confidence intervals, and number of measurements are listed in Table S1.

$$Y = \text{bottom} + (\text{top} - \text{bottom})/(1 + 10\text{^}((\text{LogIC}_{50} - X) \times \text{Hill slope})) \quad \textbf{[S1]}$$

Homology Modeling of Arrestin-1 in the Phosphopeptide-Bound Conformation. The sequences of bovine arrestin-1 and rat arrestin-2 were aligned and manually refined using Chimera (6) to adjust some of the gaps in the loop regions. The final sequence identity of the alignment was 61%. Using this alignment, peptide-bound bovine arrestin-1 (residues 10–358) was modeled with Modeller (7) using the structure of rat arrestin-2 bound to a G protein-coupled receptor phosphopeptide (8) as a template. Residues missing in the template (residues 315–317 in bovine arrestin-1) were refined using the loop optimization method in Modeller. All models were subjected to 300 iterations of variable target function method optimization and thorough molecular dynamics and simulated annealing optimization and scored using the discrete optimized protein energy potential. The 20 best-scoring models were analyzed visually, and a suitable model (in terms of low score and structure of the loops) was selected for the next step.

Molecular Docking. To create a model of the rhodopsin–arrestin-1 complex, we docked the model of peptide-bound arrestin-1 to the structure of light-activated rhodopsin (Protein Data Bank ID code 4A4M) (9). First, we manually oriented the arrestin-1 phosphosensor region close to helix 8 of rhodopsin (as the C terminus of rhodopsin, immediately after helix 8, interacts with this region of arrestin-1). We also placed the finger loop of arrestin-1 close to the crevice that opens upon activation of rhodopsin. This initial pose was refined using Rosetta (10) with a rigid-body local search around the starting position. We generated 2,500 decoys and the 50 with best scores were analyzed visually. The selected orientation (with both a low score and a suitable orientation) was subjected to an additional run of local refinement. In this stage, we generated 3,000 decoys and the best-scoring complex was selected.

Using this complex and the structure of the phosphopeptide bound to arrestin-2 (8) as templates, we then modeled the C terminus of rhodopsin in an arrestin-binding conformation using Modeller (10). The phosphopeptide present in the arrestin-2 structure is 29 residues long, but only 21 residues are solved in the crystal structure (a continuous stretch of 23 aa with a two-residue gap roughly in the middle). Because the C terminus of rhodopsin (after the palmitoylation sites in helix 8) is 25 residues long, this modeling was relatively straightforward. These two sequences were aligned in a way that the number of common phosphorylated residues was maximal.

The final resulting model of the complex between light-activated rhodopsin, including the C terminus in an arrestin-binding conformation, and active arrestin-1 was subjected to 1,000 steps of energy minimization (with the backbone atoms constrained) to optimize the geometry of the side chains and the residue–residue interactions in the protein interface.

1. Edwards PC, et al. (2004) Crystals of native and modified bovine rhodopsins and their heavy atom derivatives. *J Mol Biol* 343(5):1439–1450.
2. McDowell JH, Nawrocki JP, Hargrave PA (2000) Isolation of isoelectric species of phosphorylated rhodopsin. *Methods Enzymol* 315:70–76.
3. Vishnivetskiy SA, et al. (2007) Regulation of arrestin binding by rhodopsin phosphorylation level. *J Biol Chem* 282(44):32075–32083.
4. Spalink JD, Reynolds AH, Rentzepis PM, Sperling W, Applebury ML (1983) Bathorhodopsin intermediates from 11-cis-rhodopsin and 9-cis-rhodopsin. *Proc Natl Acad Sci USA* 80(7): 1887–1891.
5. Sun D, et al. (2013) AAscan, PCRdesign and MutantChecker: A Suite of Programs for Primer Design and Sequence Analysis for High-Throughput Scanning Mutagenesis. *PLoS ONE* 8(10):e78878.
6. Pettersen EFE, et al. (2004) UCSF Chimera—a visualization system for exploratory research and analysis. *J Comput Chem* 25(13):1605–1612.
7. Eswar N, et al. (2002) *Comparative Protein Structure Modeling Using Modeller* (John Wiley & Sons, Hoboken, NJ).
8. Shukla AK, et al. (2013) Structure of active β-arrestin-1 bound to a G-protein-coupled receptor phosphopeptide. *Nature* 497(7447):137–141.
9. Deupi X, et al. (2012) Stabilized G protein binding site in the structure of constitutively active metarhodopsin-II. *Proc Natl Acad Sci USA* 109(1):119–124.
10. Wang C, Bradley P, Baker D (2007) Protein-protein docking with backbone flexibility. *J Mol Biol* 373(2):503–519.

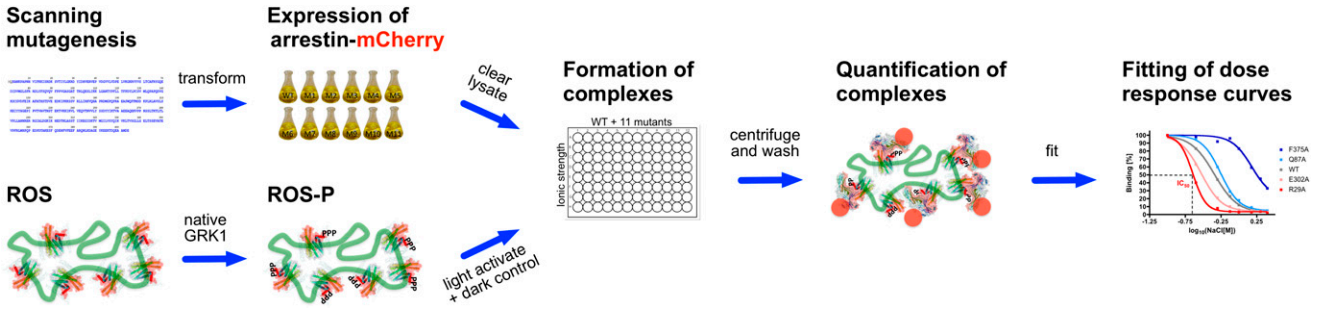

Fig. S1. Direct binding assay of arrestin–mCherry and rhodopsin in native ROS membranes. Plasmids containing arrestin mutated by scanning mutagenesis were transformed into *E. coli*. The relative expression level of each mutant with respect to the wild type was determined using fluorescence of a C-terminal mCherry fusion to arrestin. For complex formation arrestin is combined with rhodopsin in ROS membranes that had been phosphorylated with native rhodopsin kinase (GRK1). To minimize the effect of variations in the expression of different arrestin mutants, the assay contained 1.25 μM rhodopsin, far in excess of the 5–50 nM apparent binding affinity of arrestin-1 (1, 2). Consequently we observed no correlation between the amounts of functionally expressed arrestin-1 and the ability of a mutant to bind rhodopsin under increasing ionic strength. For comparison of relative binding, we combined 11 arrestin mutants and wild-type arrestin as control in a 96-well microtiter plate and probed binding to dark-state and light-activated rhodopsin in eight different salt concentrations. After centrifugation and washing steps, the amount of bound arrestin can be quantified using fluorescence of the mCherry fusion protein. The resulting data were fitted to sigmoidal dose–response curves with variable slope to extract the IC_{50} values and 95% confidence intervals listed in Table S1.

1. Bayburt TH, et al. (2011) Monomeric rhodopsin is sufficient for normal rhodopsin kinase (GRK1) phosphorylation and arrestin-1 binding. *J Biol Chem* 286(2):1420–1428.
2. Zhuang T, et al. (2013) Involvement of distinct arrestin-1 elements in binding to different functional forms of rhodopsin. *Proc Natl Acad Sci USA* 110(3):942–947.

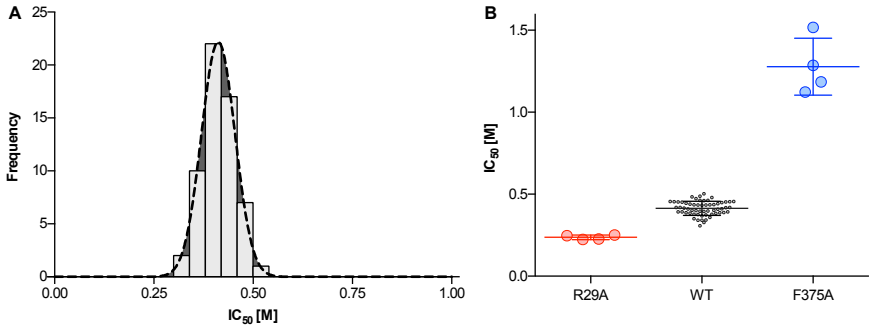

Fig. S2. Statistical analysis of IC_{50} values. (*A*) The IC_{50} of sodium chloride for arrestin–rhodopsin complex formation was derived as described in *SI Methods* and Fig. S1. The IC_{50} for complex formation with mCherry-fused wild-type arrestin was determined 59 times in independent measurements. The mean is 0.41 M with a SD of 0.04 M. The individual values were grouped in intervals with widths of 0.04 M and are shown in their frequency. The frequency distribution fitted the Gaussian model (dotted line) with an R^2 of 0.9972. (*B*) The arrestin mutants R29A and F375A, as examples for a weak (red) and a strong binder (blue), changed the IC_{50} value to 0.24 ± 0.01 M and 1.28 ± 0.17 M, respectively. IC_{50} values were determined for each mutant 4 times and 59 times for wild-type arrestin. All individual values are graphed together with mean and SD. According to Welch's *t* test, differences between mutants and wild-type arrestin are highly significant with *P* values of 0.0001 for R29A and 0.002 for F375A, respectively.

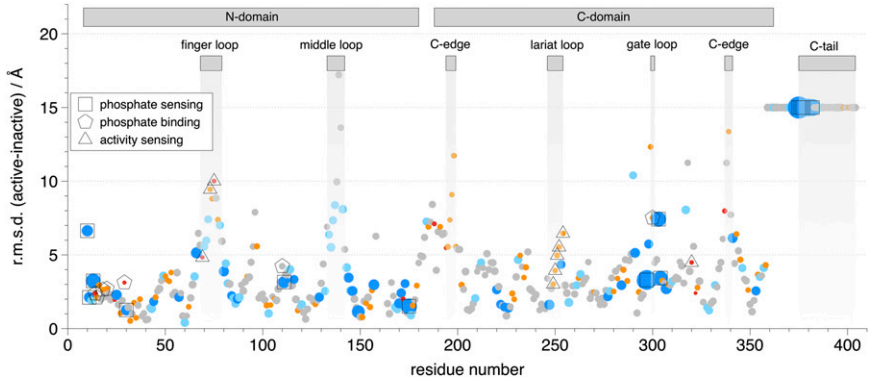

Fig. S3. Conformational changes between arrestin-1 and p44 arrestin-1. The rmsd of Cα atoms between inactive arrestin-1 (1) and preactivated p44 arrestin-1 (2) plotted against the sequence number highlight conformational changes in the arrestin loops. The C tail of arrestin is known to undergo large conformational changes upon activation (3) (here fixed to 15 Å) but had been truncated to obtain the active-state arrestin structures (4, 5). The graph shows that there is little correlation between the effect of arrestin-1 mutations on Rho-P binding (blue and large circles indicate increased binding; red and small circles indicate weak binding) and the extent of the conformational change. Residues involved in phosphosensing by the polar core and three-element interaction sites (squares), for example, range from nearly unchanged to large rearrangements above 10 Å. Similarly, residues in the arrestin loops, whose mutation strongly reduces binding to light-activated rhodopsin (triangles), undergo significant changes in case of the finger loop but only minor rearrangements in the lariat loop. In contrast, mutations in the middle loop have very little effect on binding, whereas large conformational changes occur in this region.

1. Hirsch JA, Schubert C, Gurevich VV, Sigler PB (1999) The 2.8 A crystal structure of visual arrestin: A model for arrestin's regulation. *Cell* 97(2):257–269.
2. Kim YJ, et al. (2013) Crystal structure of pre-activated arrestin p44. *Nature* 497(7447):142–146.
3. Hanson SM, et al. (2006) Differential interaction of spin-labeled arrestin with inactive and active phosphorhodopsin. *Proc Natl Acad Sci USA* 103(13):4900–4905.
4. Kim M, et al. (2012) Conformation of receptor-bound visual arrestin. *Proc Natl Acad Sci USA* 109(45):18407–18412.
5. Shukla AK, et al. (2013) Structure of active β-arrestin-1 bound to a G-protein-coupled receptor phosphopeptide. *Nature* 497(7447):137–141.

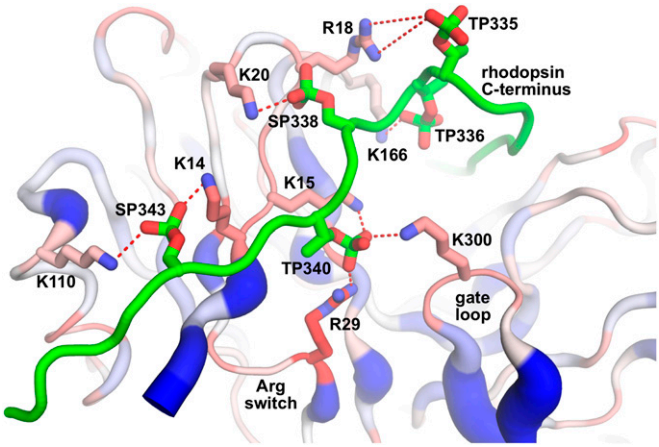

Fig. S4. Arrestin residues interacting with the phosphorylated rhodopsin C terminus. Placement of the rhodopsin C terminus along the position of the V2Rpp phosphopeptide in combination with scanning mutagenesis and binding data (blue indicates residues which increase binding; red indicates residues which decrease binding to P-ROS* upon mutation) reveals a series of positively charged arrestin residues that can interact with phosphorylated Ser and Thr residues in rhodopsin.

	TM7	helix 8	C-terminus
V2R_HUMAN	NPWIYASFS	SSVSSELRSLLCC	ARGRTPPSLGPQDESCTTASSSLAKDTSS
V2Rpp	---------	-------------	ARGRTPPSLGPQDESCTTASSSLAKDTSS
OPSD_BOVIN	NPVIYIMMN	KQFRNCMVTTLCC	GKN-PLGDDEASTTVSKTETSQVAPA---

Fig. S5. Sequence alignment of the human V2 vasopressin receptor (V2R_HUMAN), the phosphorylated peptide derived from its C terminus (V2Rpp) (1), and bovine rhodopsin (OPSD_BOVIN). The alignment includes the cytoplasmic side of TM7 (from the NPxxY motif), helix 8 for reference (defined as in the structure of rhodopsin), and the C terminus. In V2Rpp, the residues not visible in the crystal structure (4JQI) are grayed out. Phosphorylation sites are highlighted in yellow. The alignment shows that the C terminus of V2R_HUMAN and OPSD_BOVIN are very similar in length (29 and 25 residues, respectively). The C termini were aligned to maximize the overlap of phosphorylation sites.

1. Shukla AK, et al. (2013) Structure of active β-arrestin-1 bound to a G-protein-coupled receptor phosphopeptide. *Nature* 497(7447):137–141.

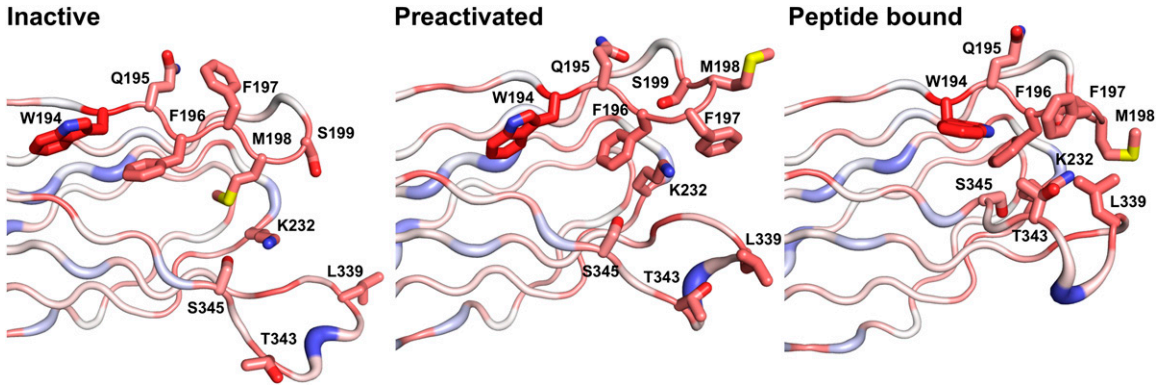

Fig. S6. Rearrangement of the arrestin C edge. The region at the edge of the C domain (C edge) contains a series of amino acids that reduce binding to P-ROS* (red) and very few with a positive effect (blue). Comparison of inactive (*Left*) (1), preactivated p44 arrestin (*Center*) (2), and a homology model of arrestin-1 based on the crystal structure of arrestin-2 bound to a receptor phosphopetide (*Right*) (3) show a reorganization of the C edge.

1. Hirsch JA, Schubert C, Gurevich VV, Sigler PB (1999) The 2.8 A crystal structure of visual arrestin: A model for arrestin's regulation. *Cell* 97(2):257–269.
2. Kim YJ, et al. (2013) Crystal structure of pre-activated arrestin p44. *Nature* 497(7447):142–146.
3. Shukla AK, et al. (2013) Structure of active β-arrestin-1 bound to a G-protein-coupled receptor phosphopeptide. *Nature* 497(7447):137–141.

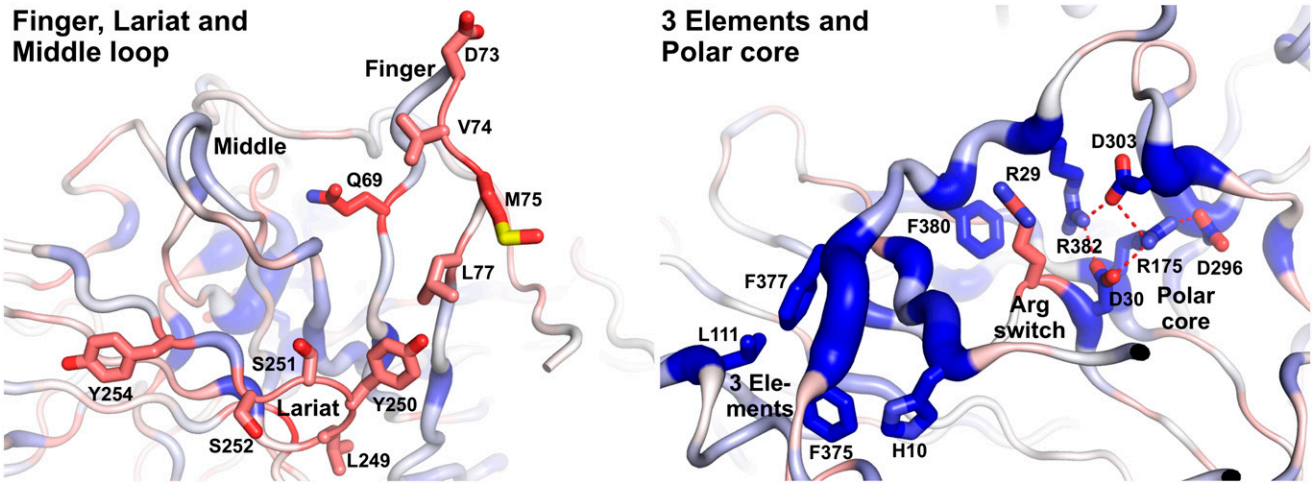

Fig. S7. Close-up of functional regions involved in binding to light-activated rhodopsin (*Left*) and phosphosensing (*Right*). Relative binding of arrestin mutants (IC_{50} values shown as increasing ribbon width and as spectrum ranging from red over white to blue) plotted on the crystal structure of arrestin-1 in the basal conformation (1).

1. Hirsch JA, Schubert C, Gurevich VV, Sigler PB (1999) The 2.8 A crystal structure of visual arrestin: A model for arrestin's regulation. *Cell* 97(2):257–269.

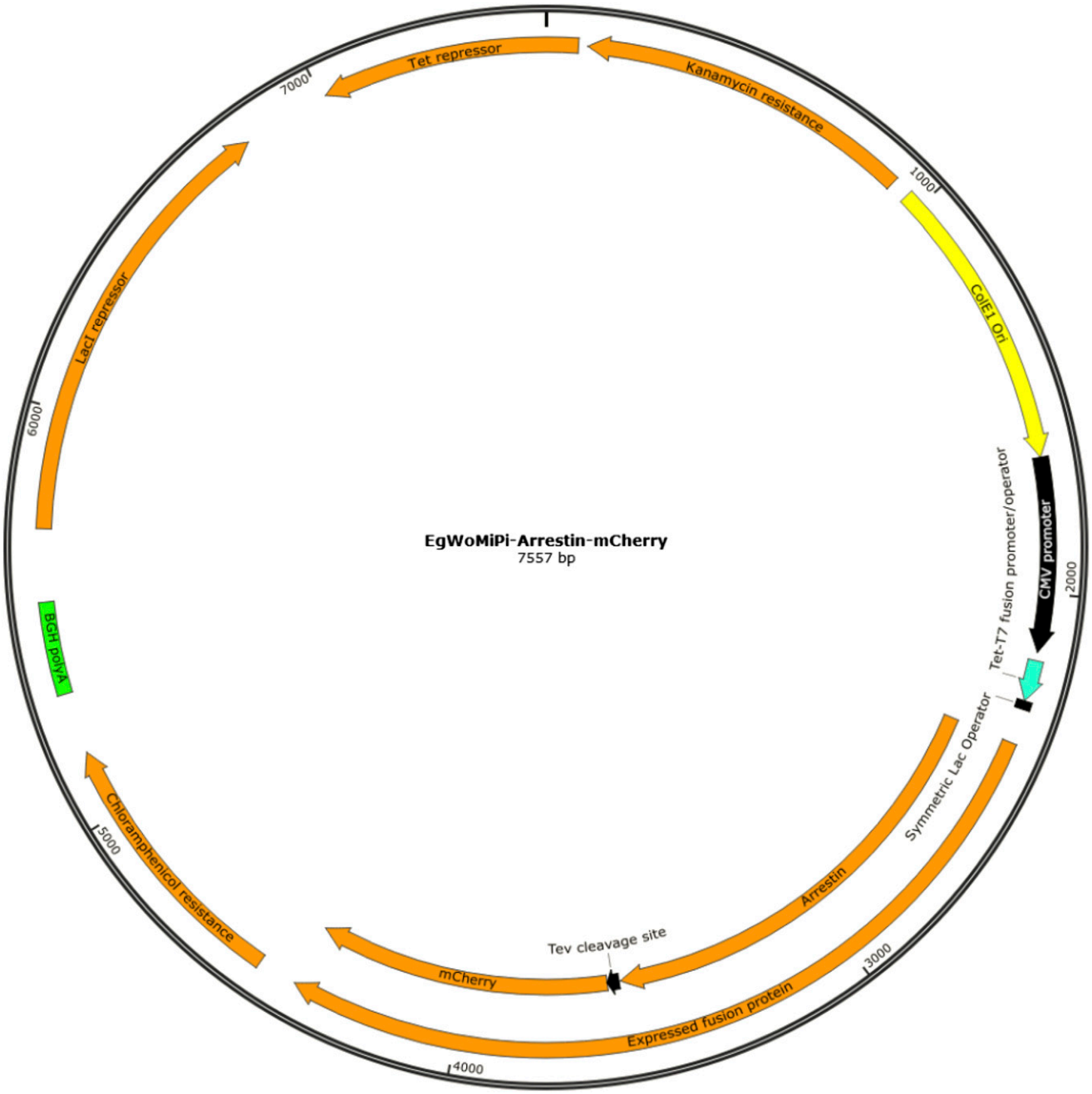

Fig. S8. The EgWoMiPi expression vector. The plasmid was designed with the aim to guarantee tightly regulated and tunable expression in most available strains of *E. coli*. In addition, expression in mammalian cells is possible under the CMV promoter that is situated upstream of a Tet operator. The inserted bovine arrestin-1 was further C-terminally extended by mCherry–His6 connected by a short linker sequence (GSSG) and a tobacco etch virus (TEV) protease cleavage site (ENLYFQGS).

Other Supporting Information Files

Table S1 (DOC)